Stereospecific Activation of the Procarcinogen Benzo[*a*]pyrene: A Probe for the Active Sites of the Cytochrome P450 Superfamily†

Jeffrey P. Jones,*,‡ Magang Shou,§ and Kenneth R. Korzekwa*,∥

Department of Pharmacology, University of Rochester, 601 Elmwood Avenue, Rochester, New York 14642, Laboratory of Molecular Carcinogenesis, National Cancer Institute, Building 37, Room 3E24, National Institutes of Health, Bethesda, Maryland 20892, and Center for Clinical Pharmacology, 623 Scaife Hall, University of Pittsburgh Medical Center, Pittsburgh, Pennsylvania 15217

Received October 17, 1994; Revised Manuscript Received February 22, 1995⊗

ABSTRACT: It has been established previously that the stereochemistry of epoxidation of the procarcinogen benzo[*a*]pyrene determines the potency of the ultimate carcinogen. Herein we report that seven human P450s, five rodent P450s, and two bacterial P450s all convert B[*a*]P to the most potent carcinogenic stereoisomer. This is in contrast to most P450-catalyzed reactions, for which the various P450 enzymes often differ in both regioselectivity and stereoselectivity. This is likely due to the large size of the substrate molecule and its constraints in the active sites. Smaller substrates that can rotate more freely in the active site may be expected to have greater variations in binding orientations and therefore greater differences in stereoselectivities. Molecular mechanics is used to determine the specific amino acids responsible for the stereochemical outcome. Molecular dynamics is then used to strengthen the hypothesis that a single helical region, one that is likely to be conserved in all P450s, plays a primary role in determining the stereoselectivity of the reaction.

The study of polycyclic aromatic hydrocarbons (PAHs) began in the 1920s with efforts to determine the structures of the carcinogenic compounds present in coal tar. The first purified chemical shown to be a carcinogen was the PAH dibenz[*a,h*]anthracene (Cook et al., 1932b). B[*a*]P was first purified from coal tar and shown to be carcinogenic in 1933 (Cook et al., 1932a) and has since become the most thoroughly studied PAH. The requirement for enzymatic activation and the elucidation of the metabolic pathways was determined with the efforts of several laboratories (Jerina, 1983; Yang et al., 1977). It is now generally accepted that B[*a*]P is metabolized by the cytochrome P450s and epoxide hydrolase to several metabolites including the carcinogenic B[*a*]P 7,8-diol 9,10-epoxide stereoisomers. The formation of the diol epoxides requires the three steps shown in Scheme 1. Previous studies with rat liver microsomes suggested that the major constitutive and inducible P450s metabolize B[*a*]P stereoselectively to the more carcinogenic 7(*R*),8(*S*)-epoxide (Levin et al., 1980; Yang, 1988). However, the structural factors responsible for the stereoselectivity of activation have not been elucidated. We now report that seven human P450s, five rodent P450s, and two bacterial P450s all metabolize B[*a*]P with similar stereoselectivity. This is the first time the stereoselectivity of B[*a*]P metabolism has been reported for either the human or bacterial enzymes. A similar stereochemical outcome is observed for all P450 enzymes. The similar experimental outcomes allow us to use the known crystal structures for the two bacterial P450 enzymes to describe the structural basis for the stereoselectivity of B[*a*]P metabolism using molecular modeling techniques. Thus, for the first time, we can provide a structural model for why the procarcinogen B[*a*]P is metabolized to the most potent diol epoxide carcinogen in man.

METHODS

Metabolism Studies. Preparation of recombinant vaccinia viruses containing the cDNAs encoding the P450 proteins m1A1, m1A2, h1A2, h2C8, h2C9, h2B6, h3A4, h2E1, rat 2A1, rat 2B1, and rabbit 4B1 were constructed as described previously (Gonzalez et al., 1991). Virus stock was prepared in human TK-143 (thymidine kinase-deficient human embryoblast) cells by infection with the recombinant vaccinia viruses for 48 h. For metabolism studies with the vaccinia virus expression system, enzymes were expressed in Hep G2 cells. These cells contain adequate cytochrome P450 reductase (1.5−4.0 times the P450 content) and an excess of cytochrome b_5. Hep G2 cells were infected with vaccinia virus with a multiplicity of infection of ~10 and after 24 h were harvested by scraping and then frozen at −80 °C until used. P450 contents were quantitated by CO difference spectra as previously described (Omura & Sato, 1964) with the additional subtraction of a difference spectra of cells infected with wild-type vaccinia virus. P450 contents ranged from 10 to 30 pmol of P450/mg of total cell protein. For metabolism, cells were thawed, sonicated (15 30% pulses), and centrifuged at 500000*g* for 10 min. The membrane fraction was resuspended in 50 mM potassium phosphate buffer and used as the enzyme source.

Metabolism with human P4501A1 used a lymphoblastoid cell expression system (Crespi, 1991) obtained from Gentest, Woburn, MA. Cells were harvested and stored at −80 °C until used. For the metabolism studies, cells were treated as above for the vaccinia expression system.

† J.P.J. acknowledges support from the DuPont Co. and NIEHS Grant ES06062.

* To whom correspondence may be addressed.
‡ Department of Pharmacology, University of Rochester.
§ Laboratory of Molecular Carcinogenesis, National Cancer Institute.
∥ Center for Clinical Pharmacology, University of Pittsburgh Medical Center.

⊗ Abstract published in *Advance ACS Abstracts,* April 15, 1995.

0006-2960/95/0434-6956$09.00/0

Scheme 1: Metabolic Pathway for the Production of the Ultimate Carcinogen of B[*a*]P[a]

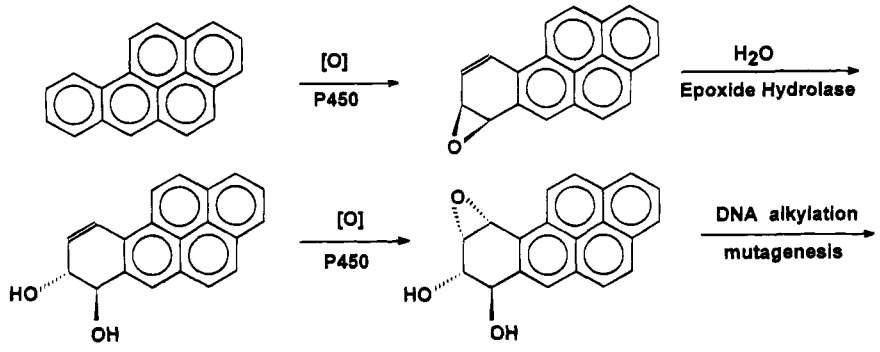

[a] The most carcinogenic diol epoxide is formed through a sequence in which B[*a*]P is first metabolized to the 7(*R*),8(*S*)-epoxide, followed by stereospecific hydration by epoxide hydrolase to the 7(*R*),8(*R*)-dihydrodiol. This dihydrodiol is further metabolized by the P450s to the two 7(*R*),8(*S*)-dihydrodiol 9,10-epoxides of which the 9(*S*),10(*R*)-epoxide is the most carcinogenic (Slaga et al., 1977).

A typical 10-mL metabolic incubation contained the membrane fraction of 10^9 AHH-1 cells (~12−15 mg of protein/mL) or 1 nmol of vaccinia-expressed P450 (only 0.1 nmol of mouse cyp1A1 was used), 10 μmol of NADPH, and 50 mM Tris-HCl buffer (pH = 7.4). For metabolism with $P450_{cam}$, the 10-mL incubations contained 7.2 nmol of enzyme, ~3 mg of microsomes of Hep G2 cells as a source of EH, 1 mM NADPH, 50 mM potassium phosphate, and 100 mM KCl buffer at pH = 7.0. $P450_{BM-3}$ was purified by the method of Narhi and Fulco (1986). For metabolism with $P450_{BM-3}$, 10-mL incubations contained 17 nmol of purified P450 and human epoxide hydrolase expressed in TK^- cells. All incubation mixtures were preincubated for 2 min at 37 °C in a shaking water bath, and reactions were initiated by addition of 200 nmol of [G-^{3}H]B[*a*]P (specific activity = 466 mCi/mmol). The incubations were terminated (usually after 30 min) by the addition of 1 volume of cold acetone. The remaining substrate and metabolites were extracted with 4 volume of ethyl acetate, vortexed, and centrifuged for 10 min at 3000 rpm (Sorvall RT600 centrifuge, Du Pont). The organic solvent extracts were evaporated at 40 °C to dryness under nitrogen. The residue was dissolved in methanol, and cold B[*a*]P dihydrodiol standards were added to radiolabeled metabolite mixture as markers for HPLC analysis. Control incubations contained membrane fractions from the following control cells: Hep G2 cells infected with wild-type vaccinia virus for the vaccinia-expressed P450s, control lymphoblastoid cells for CYP1A1, Hep G2 cells for $P450_{cam}$, or expressed epoxide hydrolase for $P450_{BM-3}$.

HPLC was performed on a Hewlett-Packard Model HP1050 liquid chromatograph equipped with a multiple wavelength detector and a Radiomatic FLO-ONE\β Model A-500 radioactivity detector. B[*a*]P metabolites were separated on a Du Pont Golden Series Zorbax ODS (C_{18}) column (4.6 mm i.d. × 25 cm, Du Pont Co., Wilmington, DE) eluted with a 80-min linear gradient from 60% methanol in water (v/v) to methanol at 1 mL/min. The retention times of 9,10-, 4,5-, and 7,8-diol were 10.1, 21.2, and 24.3 min, respectively. The three diols were identified by comparing retention times on reversed-phase HPLC with cold synthetic standards and collected for application to the chiral column. The enantiomeric pairs of 9,10-, 4,5-, and 7,8-diol collected from reversed-phase HPLC were separated on an analytical column (4.6 i.d. × 25 cm, Regis Chemical Co., Morton Grove, IL) packed with spherical 5-μm γ-aminopropylsilanized silica to which either (*S*)-*N*-(3,5-dinitrobenzoyl)-leucine (*S*-DNBL) or (*R*)-*N*-(3,5-dinitrobenzoyl)phenylglycine (*R*-DNBPG) is covalently or ionically bonded. The elution solvent was solvent A (ethanol−acetonitrile or ethanol−methanol, 2:1 v/v) in hexane. Enantiomeric pairs were resolved by chiral stationary-phase HPLC.

The identities of the metabolites were verified by absorption and CD spectra. UV−visible absorption spectra of samples in solvent were determined using a 1-cm path-length quartz cuvette with a DW2000 UV/vis scanning spectrophotometer, and CD spectra of samples were obtained using a Jasco Model 500A spectropolarimeter equipped with a Model DP500 data processor.

Molecular Modeling Studies. The development of the parameters for the protoporphyrin and the methods used for the minimization of the protein structure from the crystal structure are the same as those used for nicotine (Jones et al., 1993). A dihedral force constant of 10 was used for the CA−CA−CA−CA out of plane bend. The charges on the B[*a*]P were determined using the MNDO Hamiltonian, the ESP option in MOPAC version 6, and used the AM1 optimized geometry. The charges were corrected to approximate the HF/6-31G* charges. To allow for easy reproduction of these results, the AMBER prep files, parameter data base, topology files, and the molecular dynamics input deck will be provided by Email upon request.

B[*a*]P fits very tightly into the active site of $P450_{cam}$. Close van der Waals contacts restrict the B[*a*]P molecule to the four distinct orientations shown in Figure 1. Only small fluctuations can be observed around any of these orientations, and 90-deg rotations in either the vertical or horizontal planes relative to the heme are forbidden by steric interactions. The geometries of the four binding modes were determined as follows. B[*a*]P was placed in the active site so that positions 7, 8, 9, and 10 overlapped the previously determined binding region of the pyridine ring of (*S*)-nicotine. The other atoms were placed in positions around the pyrrolidine binding site. An initial minimization was done using the steepest descent method for 200 steps using a CA−CA−CA−CA dihedral force constant of 1.0 kcal/mol. Using this method the molecule unfolded to bind in an orientation that placed the 4,5-position close to the porphyrin iron. The dihedral force constant was increased to 10 kcal/mol and another 1500 minimization steps were taken using the conjugant gradient method of minimization. Only the B[*a*]P was allowed to move using the belly option in AMBER. The three other binding modes were produced by overlaying the ring

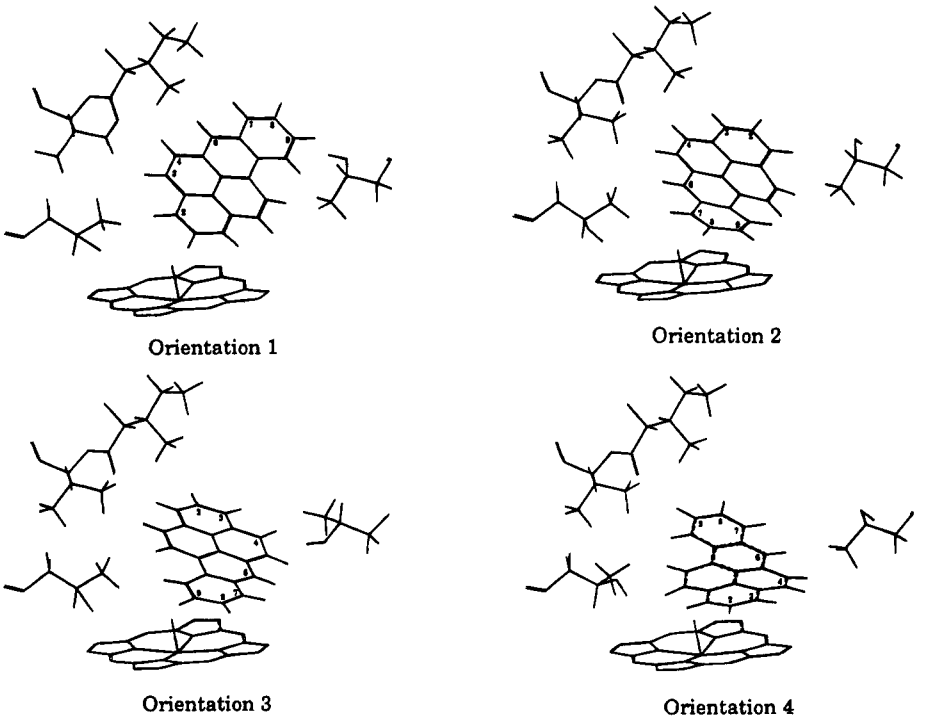

FIGURE 1: Four possible binding orientations of B[*a*]P in $P450_{cam}$. Generation of these binding orientations is discussed in the Methods section.

containing the 7,8-, 9,10-, or 1,2-positions on the ring containing the 4,5-positions in orientation 1, and 1500 steps of minimization were performed on each new binding mode.

For $P450_{BM-3}$, only the orientations similar to orientations 2 and 3 for $P450_{cam}$ were studied. For each orientation the molecule was docked by placing a force constant of 2 kcal/Å between the porphyrin Fe−O atom and either the 8- or the 10-position of B[*a*]P, and a molecular dynamics calculation was performed. After B[*a*]P was in the active site, a short minimization was performed. In this way two orientations, analogous to orientations 2 and 3 in Figure 1, were generated.

Production dynamics on $P450_{cam}$ runs were performed for 50 ps and structures saved every 200 steps. For each binding orientation, the substrate and protein were minimized for at least 2000 steps. While the fit of B[*a*]P in the active site did not allow interchange between the four different orientations, the van der Waals interactions and overall energy for each orientation were significantly negative. Furthermore, binding of the B[*a*]P molecule in each orientation could be accommodated by $P450_{cam}$ without any change in the position of the α-carbon backbone from the established crystal structure. Thus, in each minimized orientation the B[*a*]P molecule fit tightly but without any significant high-energy interactions with the protein. These minimized orientations were used for the starting coordinates for each dynamics run. Dynamics runs were performed using the AMBER program with a 1-fs time step. The belly option was used to limit the dynamics motion to the substrate and the 44 amino acids that comprise the active site. The system was warmed in 3 × 1 ps runs to 303 K. An initial 10−20 ps of dynamics was performed to equilibrate the systems. The RMS change in total energy and temperature stabilized at less than 10 kcal and 7 K, respectively, for the last 2000 steps. The RMS values of the production runs were very similar, indicating that the systems were reasonably equilibrated. No interconversion between binding orientations was observed over the entire dynamics run. If new trajectories were assigned and another 10 ps of dynamic were run, the minimized structure was nearly the same as the first minimized structure. The number of carbon−oxygen distances less than 4 Å was tabulated for each orientation during the dynamics runs. The methodology is the same as presented in Jones et al. (1993). It was assumed that if a carbon−oxygen distance was less than 4 Å, oxidation would occur at that position. Finally, to confirm that our simulations give an accurate representation of the dynamic motion of each binding orientation, we performed a second dynamics run using the structures obtained after minimization of the final structures from the first 50-ps dynamics runs and with new trajectories. The results were very similar to those from the first run. The data in Table 1 are from the sum of the multiple runs for each orientation.

RESULTS AND DISCUSSION

The metabolism of B[*a*]P by 12 different human and rodent P450s was characterized using P450s expressed in Hep G2 cells with vaccinia virus expression vectors and a lymphoblastiod cell line (Shou et al., 1994). Radiolabeled [^{3}H]B[*a*]P was incubated with membrane fractions from cells expressing the individual cytochrome P450s. All P450s produced a variety of metabolites including 4,5-, 7,8-, and 9,10-diols, 3-, 7-, and 9-phenols, and three quinones (Shou et al., 1994). The three diols are formed by the hydration of epoxides by epoxide hydrolase. Since the stereoselectivity of epoxide hydrolase is known (Levin et al., 1980; Yang, 1988), the stereochemistry of the diols can be used to determine the stereoselectivity of the P450-mediated epoxidation reactions. The diols were separated by reversed-phase HPLC and separated into individual enantiomers by chiral stationary-phase HPLC. The observed stereochemistry of the 7,8- and 9,10-diols is given in Table 1. Surprisingly, the data in Table 1 show that all 12 mammalian P450s form

Table 1: Stereoselectivity of Benzo[*a*]pyrene Metabolism by CYP Enzymes and Predicted Stereochemistry Using Molecular Dynamics

enzyme	enantiomeric ratio 9,10-diol (*RR*:*SS*)	7,8-diol (*RR*:*SS*)
CYP1A1 (human)	99.7:0.3	98.2:1.8
CYP1A1 (murine)	99.0:1.0	99.3:0.7
CYP1A2 (human)	99.8:0.2	99.2:0.8
CYP1A2 (murine)	99.1:0.9	99.1:0.9
CYP2A1 (rat)	98.6:1.4	99.5:0.5
CYP2B1 (rat)	97.9:2.1	98.6:1.4
CYP2B7 (human)	99.9:0.1	98.4:1.6
CYP2C8 (human)	97.0:3.0	80.4:19.6
CYP2C9 (human)	99.5:0.5	89.3:10.7
CYP2E1 (human)	99.1:0.9	99.1:0.9
CYP3A4 (human)	99.7:0.3	99.1:0.9
CYP4B1 (rabbit)	99.5:0.5	98.8:1.2
CYP102 (bm3)	>98:<2	>98:<2
CYP101 (cam)	98.5:1.5	97.5:2.5
CYP101 (predicted)[a]	99.0:1.0[b]	99.0:1.0[b]

[a] The combined results of the two 50-ps dynamics runs were obtained as described in the Methods section. [b] The reported values are corrected for the stereochemical outcome of epoxide opening by epoxide hydrolase (Levin et al., 1980; Yang, 1988).

the 7(*R*),8(*R*)-diol and the 9(*R*),10(*R*)-diol with an extremely high degree of stereoselectivity. Of particular importance is the fact that the 7(*R*),8(*S*)-epoxide and 9(*S*),10(*R*)-epoxide arise from attack of the active oxygen on opposite faces of the B[*a*]P.

The consistent stereochemical outcome for 7,8- and 9,10-epoxide formation by all of the enzymes in Table 1 suggests that certain structural features of the mammalian cytochrome P450s are conserved. At this time, the crystal structures of three bacterial cytochrome P450s are available (Poulos et al., 1987; Ravichandran et al., 1993; Hasemann et al., 1994). Sequence alignments along with secondary structure predictions have suggested that many of the secondary structural elements have also been preserved across the entire P450 superfamily, including the bacterial P450s (Gotoh, 1992; Nelson & Strobel, 1989). In addition, many site-directed mutagenesis studies have resulted in proposed substrate binding regions in the mammalian P450s which align with certain amino acids in the active site of $P450_{cam}$ (Johnson, 1992; Gotoh, 1992; Korzekwa & Jones, 1993). Although $P450_{cam}$ was thought to be very specific for the metabolism of camphor, it has been shown recently that other substances can serve as substrates, albeit with greatly reduced efficiency (Jones et al., 1993; Filipovic et al., 1992; Fruetel et al., 1992; Raag & Poulos, 1991). Thus, $P450_{cam}$ has been used as a model to develop hypotheses about the important steric interactions in mammalian metabolism (Jones et al., 1993).

In an attempt to determine if $P450_{cam}$ or $P450_{BM-3}$ can provide models for the stereochemical outcome of B[*a*]P metabolism, we studied the metabolism of B[*a*]P with each enzyme. Incubation of B[*a*]P with a cytochrome $P450_{cam}$ preparation and the microsomal fraction of Hep G2 cells (as a source of epoxide hydrolase) resulted in the formation of all three diols, three quinones, and two phenols. The formation of the 7,8- and 9,10-diols and 3-phenol could be completely inhibited by camphor and were not formed in the absence of the $P450_{cam}$ preparation or in the presence of hydrogen peroxide with no NADH. In contrast, some of the 4,5-diols and quinones were not inhibited by camphor, suggesting that other oxidases or nonenzymatic reactions are involved in the metabolism at these positions. The turnover number, based on camphor-inhibited activities, was lower (4.5 pmol min^{-1} $nmol^{-1}$) than for the mammalian enzymes [17−14 000 pmol min^{-1} $nmol^{-1}$ (Shou et al., 1994)]. As seen in Table 1, $P450_{cam}$ stereoselectively forms the same 7,8- and 9,10-epoxides as the mammalian P450s. Purified $P450_{BM-3}$ in the presence of expressed epoxide hydrolase was also used to metabolize B[*a*]P. Again, all three diols, three quinones, and two phenols were formed (turnover number of 24.6 pmol min^{-1} $nmol^{-1}$), with both the 7,8- and 9,10-diol formation completely inhibited by 20 μM laurate. The results reported in Table 1 indicate that the enzyme is completely stereoselective for epoxide formation at the 7,8- and 9,10-positions. To our knowledge this is the first report of either $P450_{cam}$ or $P450_{BM-3}$ metabolizing aromatic substrates.

These surprising results suggest that the bacterial crystal structures may be helpful in elucidating the steric factors responsible for the stereoselectivity of the mammalian metabolism of B[*a*]P. Thus, we docked B[*a*]P in the active sites of both $P450_{cam}$ and $P450_{BM-3}$ to determine what structural features were responsible for the stereoselectivity of the reactions.

Results of the docking experiments suggest that B[*a*]P fits very tightly into the active site of $P450_{cam}$. Close van der Waals contacts restrict the B[*a*]P molecule to four distinct orientations. Only small fluctuations can be observed around any of these orientations, and 90-deg rotations in either the vertical or horizontal planes relative to the heme are forbidden by steric interactions. The residues that have significant van der Waals contact with B[*a*]P are Pro86, Phe87, Tyr96, Thr101, Leu244, Val247, Gly248, Thr252, Ile395, and Val396 (Figure 1). Residues 86 and 87 are just prior to the B′-helix. Tyr96, the amino acid that hydrogen bonds to the carbonyl oxygen of camphor, forms the top of the B[*a*]P binding site along with Phe86. Residue 101 acts as the main contact point of the enzyme on the edge of the B[*a*]P opposite the oxidation site and is shown in Figures 1 and 2. The van der Waals contacts with Ile395 and Val396 that comprise the turn in the β5 sheet are also shown in Figure 1. Residues 244, 247, 248, and 252 are in the I-helix and act to hold the B[*a*]P molecule close to the heme oxygen. Residue 252 is particularly important in that it prevents the translation of the B[*a*]P molecule in orientation 2 to a position that would give the 9,10-oxide (Figure 2). Thr252 also prevents the translation of the B[*a*]P molecule in orientation 3 to a position that would give the 7,8-oxide (Figure 2). Thus, the interaction with the I-helix may determine the stereochemistry of epoxidations.

Two orientations, similar to those hypothesized to be responsible for 7,8- and 9,10-epoxidation in $P450_{cam}$, were studied for $P450_{BM-3}$. Strikingly similar results were observed when B[*a*]P was docked in the active site of $P450_{BM-3}$ as compared with $P450_{cam}$. When docked to $P450_{BM-3}$, both of the orientations that were studied had close steric interactions with Ser72, Leu75, Phe87, Ala264, Thr268, and Leu437. These amino acids correspond closely with the regions found to be important in $P450_{cam}$ binding. Amino acids 72, 75, and 87 are in the B′-helical region. However, Phe87 is after the B′-helix in $P450_{BM-3}$, while this residue number in $P450_{cam}$ is just prior to the B′-helix. Amino acids 264 and 268 are in the I-helix, and amino acid 437 is in a turn in the β sheet in the same spatial orientation as residues 395 and 396 which form a β turn in $P450_{cam}$. Similarly, the

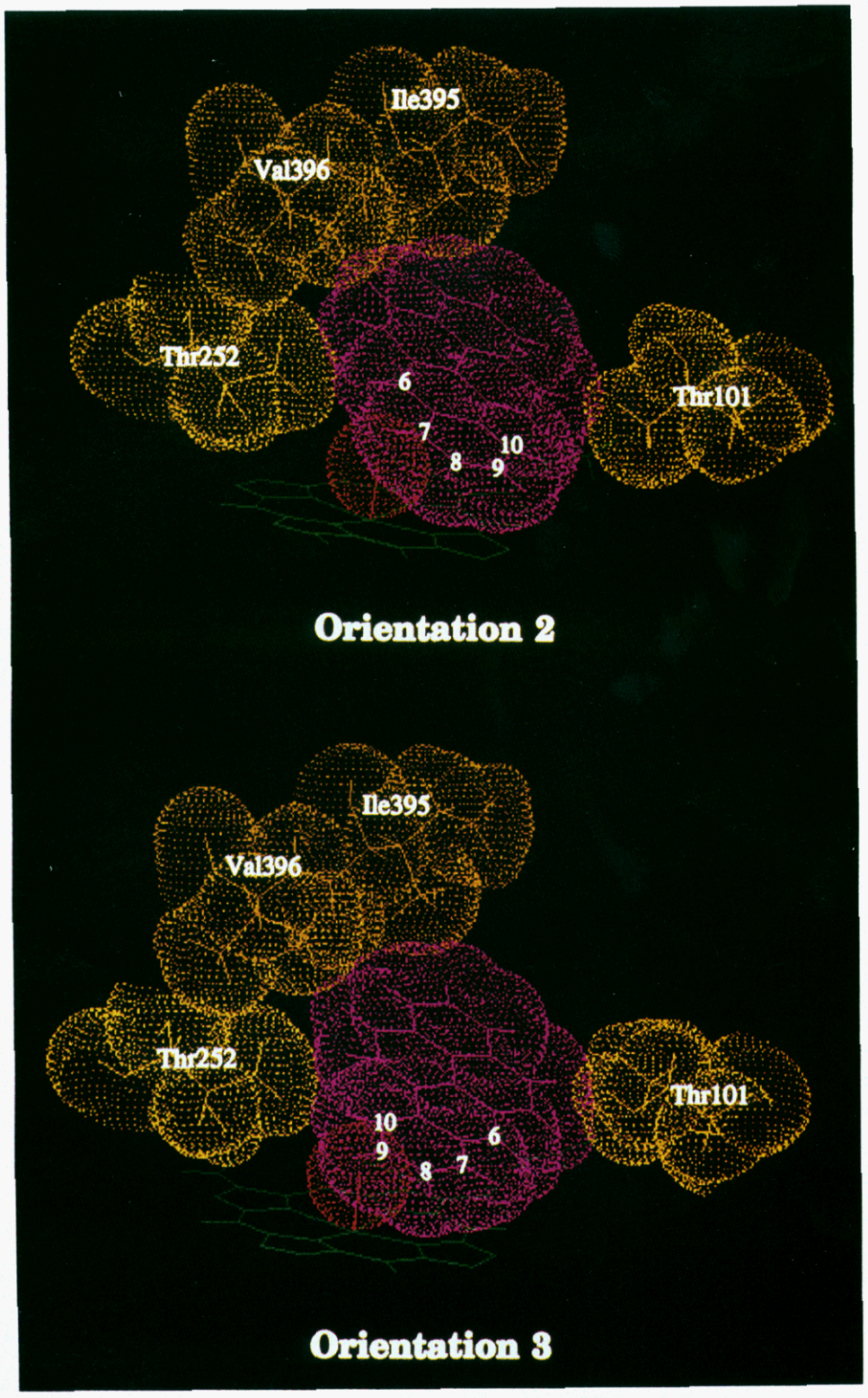

FIGURE 2: Close van der Waals contacts that prevent oxide formation at the 9,10-position for orientation 2 and oxide formation at the 7,8-position for orientation 3. These close contacts restrict epoxide formation to only one face of the B[*a*]P molecule at each position and dictate the stereochemical outcome of oxidation.

steric interactions between Ala264 and Thr268, which are in the I-helix of $P450_{BM-3}$, prevent the translation of the B[*a*]P molecule to positions that would favor formation of the epoxide that would result in the formation of the *S*,*S*-diol at either the 7,8- or 9,10-position. Finally, if constraints were placed on either orientation, such that it would pull the less favored positions into close proximity to the Fe−O species, a large increase (>50 kcal) in energy was observed during the dynamics run. One difference between $P450_{cam}$ and $P450_{BM-3}$ is that, for B[*a*]P to bind to $P450_{BM-3}$, Phe87 must rotate 90°. This places Phe87 in a position where the amino acid can provide a π-stacking interaction with the aromatic B[*a*]P. However, it would appear that, as with $P450_{cam}$, $P450_{BM-3}$ dictates the stereoselective metabolism of B[*a*]P by precluding the formation of the 7(*S*),8(*R*)- and 9(*R*),10(*S*)-epoxides. For both isoforms, unfavorable steric interactions

with the I-helix impede the formation of the epoxides which lead to the *S,S*-diol products.

While the molecular mechanics fit of the B[*a*]P molecule into the active sites is very compelling evidence for the qualitative interactions responsible for the stereoselectivity of the bacterial P450s, quantitative agreement between the computationally predicted stereochemistry and the experimental outcome was also pursued. We performed a series of dynamics runs with B[*a*]P in the $P450_{cam}$ active site. The results for the predicted diol stereochemistry are given in the last entry in Table 1. The computational results are almost identical to the experimental results. Thus, it appears that both a qualitative and a quantitative relationship exists between the computational model and the experimental results. However, it should be noted that a limited number of amino acids within the $P450_{cam}$ protein were allowed to move during the dynamics calculations. Since these results were not compared to results with an increased number of dynamically movable amino acids, we cannot be sure that certain dynamic motions of the substrate have not been artifically excluded.

Reports from many laboratories have suggested that at least some features of the tertiary structures of the P450s have been conserved throughout the superfamily. Analyses of the bacterial P450 crystal structures have provided valuable information on both the functional significance of the bacterial protein domains and their relevance to the mammalian P450 structures (Poulos, 1991; Ravichandran et al., 1993; Hasemann et al., 1994). Perhaps the most convincing evidence that some aspects of the active site are conserved by the mammalian enzymes is provided by site-directed mutagenesis studies (Gotoh, 1992; Johnson, 1992; Korzekwa & Jones, 1993). It has been reported that substrate specificity is altered by changing as few as one amino acid in a member of the P450 2 family (Lindberg & Negishi, 1989). In the studies reported here we extend our understanding of how the mammalian P450 enzymes and the bacterial $P450_{cam}$ interact with substrates. The similarities in the metabolic profiles suggest that the core structures of the P450s are similar. The similar stereoselectivity across families is unusual and is likely due to the large size of the substrate molecule and its constraints in the active sites. Smaller substrates that can rotate more freely in the active site may be expected to have greater variations in binding orientations and therefore greater differences in stereoselectivities.

In conclusion, we have presented the first description of specific apoprotein interactions that are important in determining product stereoselectivity of the prochiral procarcinogen B[*a*]P. The results of experimental and theoretical studies with the bacterial P450s suggest that the helix that is important for heme binding and catalysis is also involved in determining product stereoselectivity. The extension of the factors that influence stereoselectivity to the P450 family as a whole is supported by the fact that all the P450 enzymes that were studied show nearly identical stereoselectivity. Thus, even though the ancestral gene common to $P450_{cam}$ and mammalian P450s diverged more than three billion years ago (Nebert & Nelson, 1991), key structural and catalytic elements appear to be conserved within the P450 superfamily.

ACKNOWLEDGMENT

We gratefully acknowledge Dr. Frank Gonzalez for providing the vaccinia virus vectors and Drs. Harry Gelboin and William Trager for carefully reviewing the manuscript.

REFERENCES

Cook, J. W., Hewett, C. L., & Hieger, I. (1932a) *J. Chem. Soc.*, 395.
Cook, J. W., Hieger, E. L., Kennaway, E. L., & Mayneord, W. V. (1932b) *Proc. R. Soc. London, B 111*, 455.
Crespi, C. L. (1991) *Methods Enzymol. 206*, 123.
Filipovic, D., Paulsen, M. D., Loida, P. J., Sligar, S. G., & Ornstein, R. L. (1992) *Biochem. Biophys. Res. Commun. 189*, 488.
Fruetel, J. A., Collins, J. R., Camper, D. L., Loew, G. H., & Ortiz de Montellano, P. R. (1992) *J. Am. Chem. Soc. 114*, 6987.
Gonzalez, F. J., Aoyama, T., & Gelboin, H. V. (1991) *Methods Enzymol. 206*, 85.
Gotoh, O. (1992) *J. Biol. Chem. 267*, 83.
Hasemann, C. A., Ravichandran, K. G., Peterson, J. A., & Deisenhofer, J. (1994) *J. Mol. Biol. 236*, 1169.
Jerina, D. M. (1983) *Drug Metab. Dispos. 11*, 1.
Johnson, E. F. (1992) *Trends Pharmacol. Sci. 13*, 122.
Jones, J. P., Trager, W. F., & Carlson, T. J. (1993) *J. Am. Chem. Soc. 115*, 381.
Korzekwa, K. R., & Jones, J. P. (1993) *Pharmacogenetics 3*, 1.
Levin, W., Buening, M. K., Wood, A. W., Chang, R. L., Kedzierski, B., Thakker, D. R., Boyd, D. R., Gadaginamath, G. S., Armstrong, R. N., Yagi, H., Karle, J. M., Slaga, T. J., Jerina, D. M., & Conney, A. H. (1980) *J. Biol. Chem. 255*, 9067.
Lindberg, R. L. P., & Negishi, M. (1989) *Nature 339*, 632.
Narhi, L. O., & Fulco, A. J. (1986) *J. Biol. Chem. 261*, 7160.
Nebert, D. W., & Nelson, D. R. (1991) in *Methods in Enzymology* (Waterman, W. R., & Johnson, E. F., Eds.) Vol. 206, pp 3−11, Academic Press, San Diego.
Nelson, D. R., & Strobel, H. W. (1989) *Biochemistry 28*, 656.
Omura, T., & Sato, R. (1964) *J. Biol. Chem. 239*, 2370.
Poulos, T. L. (1991) *Methods Enzymol. 206*, 11.
Poulos, T. L., Finzel, B. C., & Howard, A. J. (1987) *J. Mol. Biol. 195*, 687.
Raag, R., & Poulos, T. L. (1991) *Biochemistry 30*, 2674.
Ravichandran, K. G., Boddupalli, S. S., Hasemann, C. A., Peterson, J. A., & Deisenhofer, J. (1993) *Science 261*, 731.
Shou, M., Korzekwa, K. R., Crespi, C. L., Gonzalez, F. J., & Gelboin, H. V. (1994) *Mol. Carcinog. 10*, 159.
Slaga, T. J., Bracken, W. M., Viaje, A., Levin, W., Yagi, H., Jerina, D. M., & Conney, A. H. (1977) *Cancer Res. 37*, 4130.
Yang, S. K. (1988) *Biochem. Pharmacol. 37*, 61.
Yang, S. K., McCourt, D. W., Leutz, J. C., & Gelboin, H. V. (1977) *Science 196*, 1199.

BI9424050